Quantum susceptance and its effects on the high-frequency response of superconducting tunnel junctions

Qing Hu,* C. A. Mears, and P. L. Richards
Department of Physics, University of California, and Materials and Chemical Sciences Division, Lawrence Berkeley Laboratory, Berkeley, California 94720

F. L. Lloyd†
Electromagnetic Technology Division, National Institute of Standards and Technology, Boulder, Colorado 80303
(Received 16 July 1990)

We have made the first direct measurement of the quantum susceptance that arises from the nondissipative part of quasiparticle tunneling in a superconductor-insulator-superconductor tunnel junction. The junction is coupled to an antenna and a superconducting microstrip stub to form a resonator; the resonant frequency is determined from the response of the junction to broadband radiation from a Fourier-transform spectrometer. A 19% shift of the resonant frequency, from 73 to 87 GHz, is observed, which arises from the change of the quantum susceptance of the junction with dc bias voltage. This shift is in excellent agreement with calculations based on the Werthamer-Tucker theory, which includes the quantum susceptance. We also demonstrate that it is essential to include the quantum susceptance in our theoretical computation to explain the photon-assisted-tunneling steps, which have negative dynamic conductance. Such steps are observed when the junction is pumped at slightly below the resonant frequency of the capacitor and the stub. The quantum susceptance should exist in all tunnel devices whose nonlinear I-V characteristics are due to elastic tunneling.

I. INTRODUCTION

Tunneling is a quantum-mechanical phenomenon. One of the consequences of such processes is that the current-voltage relation is usually not instantaneous in the presence of an ac drive, provided the driving frequency is higher than the inverse of the lifetimes of the eigenstates involved. This noninstantaneous current-voltage relation consequently gives rise to a reactive component[1–4] of the tunneling current in addition to a dissipative, resistive one. If the tunneling processes are elastic, then the I-V curve contains direct information about the density of states in the two sides of the junction. In this case, the resistive (dissipative) tunneling is given by the dc I-V curve of a tunnel junction. The reactive (nondissipative) component is related to the resistive component through a frequency Kramers-Kronig transformation, as required for any causal, linear response.[5] Therefore, the high-frequency response of the junction can be completely deduced from the dc I-V curve. Consequently, the frequency-dependent conductance which is associated with a nonlinear elastic tunneling I-V curve should give rise to a susceptance. The subject of this paper is the effect of this susceptance, called quantum susceptance herein, on the response of superconductor-insulator-superconductor (SIS) junctions to high-frequency radiation.

It is well known that there are two types of charge carriers that tunnel across a SIS junction: Cooper pairs and quasiparticles. They arise from the superconducting condensate and the excitations, respectively. Due to the noninstantaneous current-voltage relation, the tunneling current from each carrier contains two components in the presence of an ac drive. The in-phase component is dissipative (resistive) while the out-of-phase one is nondissipative (reactive). For Cooper-pair tunneling current, the in-phase component is the Josephson $\cos\phi$ term,[1,2,6] while the out-of-phase component is the Josephson $\sin\phi$ term.[1,2,6] For quasiparticles, the in-phase component is given by the dc quasiparticle I-V characteristic, while the out-of-phase component is the quantum susceptance or quantum reactance.[1–4] The reactive quasiparticle tunneling current is a result of quantum sloshing. If the energy difference of the initial and final states on two sides of the junction is different from the photon energy, no photon-assisted tunneling can take place. Instead, the quasiparticles slosh back and forth between the two sides by absorbing and then emitting photons of the same frequency.

Werthamer derived an expression for the response function of both Cooper pairs and quasiparticles.[1] The real parts of the response functions correspond to the reactive components of the tunneling currents, and the imaginary parts correspond to the resistive components. Using Werthamer's theory, Harris[2] analyzed the response of a SIS junction to a rf radiation in the small-signal limit. He correctly predicted the effect of the quantum susceptance at zero dc bias voltage. While Josephson tunneling and quasiparticle resistive tunneling have been extensively studied, quantum susceptance has been largely ignored. This is because the contribution from the quantum susceptance to the tunneling current is only significant at frequencies high enough that the voltage as-

sociated with a quantum of radiation, $V=\hbar\omega/e$, is larger than the voltage scale on which the I-V characteristic of a SIS junction is nonlinear.[3] Josephson-effect devices originally showed greater promise as useful high-frequency devices, so the effects of both $\sin\phi$ and $\cos\phi$ terms on the response of Josephson junctions have been studied extensively.[7,8] The quasiparticle tunneling was originally studied as a measure of the density of states for excitations. This measurement is done essentially at zero frequency so the quantum susceptance makes no contribution. This situation has changed since the invention of SIS quasiparticle direct detectors and SIS quasiparticle mixers which utilize quasiparticle tunneling for high-frequency operation. Tucker[3] first studied the reactive quasiparticle tunneling at arbitrary dc and rf bias voltages. He predicted that a SIS mixer which has a noninstantaneous current-voltage relation may have a mixer gain greater than unity. In contrast, a classical resistive mixer, whose current-voltage relation is instantaneous, has a maximum mixer gain of unity.[9] It was speculated that this mixer gain is due to a parametric amplification from the nonlinear quantum susceptance. However, a detailed analysis[10] indicated that the effect of the quantum susceptance is quite subtle and is not responsible for the predicted mixer gain. It was further argued that, like the Josephson $\cos\phi$ term,[11] the quantum susceptance should be difficult to detect experimentally.

In this paper, we report experimental evidence for the quantum susceptance from a measurement of a shift of the resonant frequency of a superconducting microstrip stub resonator which contains a SIS junction. This shift of the resonant frequency is due to the change of the quantum susceptance as a function of dc bias voltage. We also present an analysis of dc I-V curves of a SIS junction pumped with sufficient rf power so that the photon-assisted-tunneling steps are clearly seen. In an earlier work, we demonstrated that the quantum susceptance is essential to the explanation of the negative photon-assisted-tunneling steps observed when the junction is pumped at frequencies slightly below the resonant frequency.[12] This paper is organized as follows: the theoretical background will be introduced in Sec. II, the experimental details will be described in Sec. III, the comparison between the theory and the experiments will be discussed in Sec. IV, and finally the conclusion will be drawn in Sec. V.

II. THEORETICAL BACKGROUND

Based on a perturbation theory using a tunneling Hamiltonian,[6,13] Werthamer[1] derived an expression for the tunneling current as a function of time in the presence of both dc and ac bias:

$$I(t)=\mathrm{Im}\int\int d\omega\, d\omega'[W(\omega)W^*(\omega')e^{-i(\omega-\omega')t}j_{\mathrm{qp}}(\omega'+eV_0/\hbar)+W(\omega)W(\omega')e^{-i(\omega+\omega')t+i\phi}j_p(\omega'+eV_0/\hbar)]\ , \tag{1}$$

where j_{qp} and j_p are the response functions of quasiparticles and Cooper pairs, respectively. The first term in Eq. (1) is the quasiparticle tunneling current. The second term is the pair tunneling current which depends on the phase difference ϕ between the superconducting ground-state wave functions on the two sides of the junction. The real parts of the response functions correspond to the reactive components, and the imaginary parts correspond to the resistive components. $W(\omega)$ is the Fourier frequency component of the time-varying phase factor caused by the ac bias voltage:

$$\exp\left[-i\frac{e}{\hbar}\int^t dt'[V(t')-V_0]\right]=\int_{-\infty}^{\infty}d\omega\, W(\omega)e^{-i\omega t}\ . \tag{2}$$

For BCS-like superconductors, j_{qp} and j_p can be calculated using the density of states of quasiparticles and Cooper pairs. However, the calculation is quite complicated.[1] The following shows that the quasiparticle response function j_{qp} can be measured directly from the dc I-V curve. When the bias voltage $V(t)$ contains only a dc component V_0, then $W(\omega)=\delta(0)$, and from Eq. (1) we have

$$I(t)=\mathrm{Im}[j_{\mathrm{qp}}(\omega_0)]+\mathrm{Re}[j_p(\omega_0)]\sin\phi+\mathrm{Im}[j_p(\omega_0)]\cos\phi\ , \tag{3}$$

where $\omega_0=eV_0/\hbar$. Since both the $\sin\phi$ and $\cos\phi$ terms oscillate at the Josephson frequency $\omega_J=2eV_0/\hbar$, the only dc component in Eq. (3) is the first term. Therefore, $\mathrm{Im}[j_{\mathrm{qp}}(eV_0/\hbar)]$ is equal to the dc quasiparticle I-V curve $I_{\mathrm{dc}}(V_0)$.

$$\mathrm{Im}[j_{\mathrm{qp}}(\omega_0)]=I_{\mathrm{dc}}(V_0)\ . \tag{4}$$

Equation (4) implies that the imaginary part of the quasiparticle response function at frequency $\omega_0=eV_0/\hbar$ is equal to the dc tunneling current at bias voltage V_0. Because of the absence of $\mathrm{Re}[j_{\mathrm{qp}}(\omega_0)]$ in Eq. (3), it is clear that the reactive part of the quasiparticle response function has no contribution to the tunneling current when the bias voltage is time independent. In contrast to the quasiparticle response function, both the real and imaginary parts of the pair response function contribute to the tunneling current at dc bias. The real part of j_p gives rise to the familiar Josephson $\sin\phi$ term, while the imaginary part of j_p gives the Josephson $\cos\phi$ term.

The real and imaginary parts of both quasiparticle and Cooper-pair response functions are related through a frequency Kramers-Kronig transform, as required by any causal and finite response. For $j_{\mathrm{qp}}(\omega)$,[3]

$$\mathrm{Re}[j_{qp}(\omega)]=P\int_{-\infty}^{\infty}\frac{d\omega'}{\pi}\frac{\mathrm{Im}[j_{qp}(\omega')]-\hbar\omega'/eR_n}{\omega'-\omega}$$
$$=I_{KK}(V)$$
$$=P\int_{-\infty}^{\infty}\frac{dV'}{\pi}\frac{I_{dc}(V')-V'/R_n}{V'-V}\ . \qquad (5)$$

In Eq. (5), we have used Eq. (4) to replace $\mathrm{Im}[j_{qp}(\omega')]$ with $I_{dc}(V')$, $eV'/\hbar=\omega'$, and $eV/\hbar=\omega$. We subtract an ohmic term from the quasiparticle I-V curve to prevent divergence of the integral. This is allowed because only the nonlinear portion of $I_{dc}(V)$ gives rise to a reactive component. The frequency-independent ohmic response corresponds to an instantaneous current-voltage relation and thus does not contribute to the reactive component. It can be shown from Eq. (1) that all measurable quantities depend only on differences between values of $I_{KK}(V)$ and not on its absolute magnitude. In Figs. 1(a) and 1(b), we plot an experimentally measured I-V curve of a SIS junction and the voltage Kramers-Kronig transform calculated from Eq. (5). The peak of K_{KK} at the gap voltage V_g corresponds to the sharp nonlinearity of the dc I-V curve $I_{dc}(V)$ at V_g. At $T=0$, for an ideal SIS junction whose quasiparticle density of states is given by the BCS theory, the peak in I_{KK} diverges logarithmically at V_g.[1-4]

Equations (4) and (5) suggest a very powerful way of deducing the frequency-dependent response function of quasiparticles. The dc current $I_{dc}(V)$ as a function of dc bias voltage gives the imaginary part of the response function as a function of frequency; its voltage Kramers-Kronig transform gives the real part of the response function. Therefore, the dc I-V curve, which can be easily measured, contains all the information about the response of the quasiparticles in a SIS junction at high frequencies. Two conditions must be satisfied for this statement to be valid. First, the quasiparticle tunneling must be elastic within the tunnel barrier so that the dc I-V curve gives direct information about the density of states of the quasiparticles in the two sides of the junction. Second, tunneling probability must be small enough so that the tunneling does not significantly change the density of states on either side. These two conditions are met for SIS junctions with modest current densities $\lesssim 10^4$ A/cm^2 and high-quality tunnel barriers which are free from impurities and imperfections.

We will focus on the quasiparticle tunneling in this paper. The effect of the Cooper pairs can be minimized either by applying a magnetic field, or by biasing the SIS junction at a voltage high enough that the Josephson current oscillates at a frequency high enough to be effectively shunted by the junction capacitance. In the presence of a time-dependent bias voltage,

$$V(t)=V_0+V_\omega\cos\omega t\ ,$$

the quasiparticle tunneling current as a function of time is given by[3]

$$I(t)=a_0+\sum_{m=1}^{\infty}[2a_m\cos(m\omega t)+2b_m\sin(m\omega t)]\ . \qquad (6)$$

The coefficients of the current at ω and its harmonics are given by

$$2a_m=\sum_{n=-\infty}^{\infty}J_n(\alpha)[J_{n+m}(\alpha)+J_{n-m}(\alpha)]I_{dc}(V_0+n\hbar\omega/e)\ ,$$
$$2b_m=\sum_{n=-\infty}^{\infty}J_n(\alpha)[J_{n+m}(\alpha)-J_{n-m}(\alpha)]I_{KK}(V_0+n\hbar\omega/e)\ . \qquad (7)$$

Here, I_{dc} and I_{KK} are the same as in Eqs. (4) and (5), J_n is the nth Bessel's function, and $\alpha=eV_\omega/\hbar\omega$ is the dimensionless rf voltage. Equations (6) and (7) indicate that many harmonics of the drive frequency ω exist in a SIS junction. The amplitudes of these current components have a nonlinear dependence on the rf drive voltage V_ω. Equations (6) and (7) also indicate that there exists an out-of-phase reactive component $\sin\omega t$ as well as an in-phase component $\cos\omega t$. We will show later that the current amplitude of the two components can be comparable. It should be noted that the dc I-V curve $I_{dc}(V_0)=a_0$ of a voltage-pumped SIS junction is completely independent of the real part of the quasiparticle response function I_{KK}. Therefore, $\mathrm{Re}(j_{qp})$ cannot be measured from the dc I-V curves of a voltage-pumped SIS junction. This is in contrast to the pair-response function, whose real part $\mathrm{Re}(j_p)$ (Josephson $\sin\phi$ term)

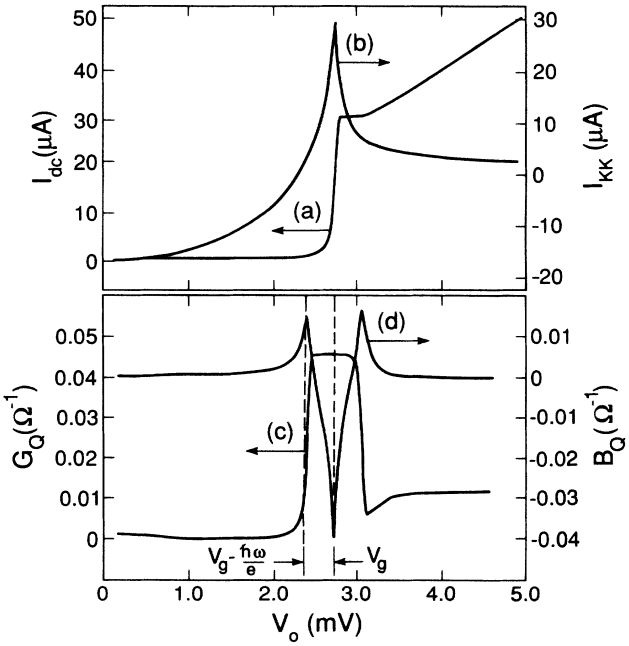

FIG. 1. (a) Measured dc I-V curve of the SIS junction studied in this paper, the junction temperature is about 4.5 K. (b) Kramers-Kronig transform of the I_{dc} calculated using Eq. (5). (c) Quantum conductance G_Q at $\omega/2\pi=77$ GHz calculated from Eq. (8a) using the $I_{dc}(V)$ in Fig. (a). (d) Quantum susceptance B_Q at 77 GHz calculated from Eq. (8b) using the I_{KK} in (b).

contributes to a dc current at some discrete voltages which correspond to Shapiro's steps. From the width of those Shapiro's steps as functions of rf voltage amplitude, $\mathrm{Re}(j_p)$ can be measured as a function of frequency.[14]

The analysis of the response of quasiparticle tunneling current to a large-amplitude rf radiation is very complicated since multiphoton nonlinear processes are involved. In general, numerical computation is required and it is difficult to gain an intuitive understanding of the physics involved. However, in the small signal limit $\alpha \ll 1$, only the one-photon process is significant, so the problem is linear. If we define an admittance $Y_Q(\omega)$ as the ratio of the induced rf quasiparticle current and the rf voltage $Y_Q(\omega)=I_\omega/V_\omega$, then, from Eqs. (6) and (7) to the leading order of α, the real and imaginary parts of $Y_Q(\omega)$ are given by

$$G_Q(\omega)=\mathrm{Re}[Y_Q(\omega)]$$
$$=\frac{e}{2\hbar\omega}[I_{\mathrm{dc}}(V_0+\hbar\omega/e)-I_{\mathrm{dc}}(V_0-\hbar\omega/e)]\ , \quad (8a)$$
$$B_Q(\omega)=\mathrm{Im}[Y_Q(\omega)]$$
$$=\frac{e}{2\hbar\omega}[I_{\mathrm{KK}}(V_0+\hbar\omega/e)-2I_{\mathrm{KK}}(V_0)+I_{\mathrm{KK}}(V_0-\hbar\omega/w)]\ . \quad (8b)$$

G_Q and B_Q are called quantum conductance and quantum susceptance, respectively, in this paper and in a previous work.[15] In the limit of low frequency, the quantum conductance $G_Q(\omega)$ reduces to the classical limit dI/dV as expected for any system whose characteristic frequency is much higher than the driving frequency. In the limit of high frequency, $G_Q(\omega)$ approaches the inverse of the normal-state resistance $1/R_n$ at frequencies far above the gap frequency. This implies that the response of a SIS junction is like a classical diode at low frequencies and becomes ohmic when the photon energy is much greater than the gap energy. In a previous work,[15] we showed that the quantum conductance G_Q and the quantum susceptance B_Q defined in Eqs. (8a) and (8b) are related through a frequency Kramers-Kronig transform, as required for any causal, linear response,[5]

$$B_Q(\omega)=P\int_{-\infty}^{\infty}\frac{d\omega'}{\pi}\frac{G_Q(\omega')}{\omega'-\omega}\ . \quad (9)$$

This approach is simpler than the one we used here. However, in this paper, we are interested in the case of arbitrary signal strength, so we started with Eqs. (6) and (7) which apply to the general case.

Expression (8b) for the quantum susceptance B_Q can be interpreted geometrically. $B_Q(\omega)$ is a measure of the curvature of the three points $I_{\mathrm{KK}}(V_0+\hbar\omega/e)$, $I_{\mathrm{KK}}(V_0)$, and $I_{\mathrm{KK}}(V_0-\hbar\omega/e)$. When the curvature is upward, B_Q is positive and capacitive, when the curvature is downward, B_Q is negative and inductive. It can be seen from Fig. 1(b) that, as we change the dc bias voltage V_0 from zero, the curvature of I_{KK} changes from positive to negative and back to positive. This implies that the quantum susceptance changes from capacitive to inductive and back to capacitive as shown in Fig. 1(d). B_Q has the largest capacitive value at one-photon voltage $\hbar\omega/e$ below the gap voltage V_g and the largest inductive value at V_g. In Fig. 1(c), we also plot the quantum conductance G_Q as a function of bias voltage. G_Q is largely only within one-photon voltage $\hbar\omega/e$ below and above V_g, which corresponds to the voltage where a quasiparticle can tunnel to the other side by absorbing or emitting one photon.

It is easy to understand that the quantum conductance G_Q comes from the photon-assisted tunneling. It is less straightforward that the quantum susceptance B_Q comes from a sloshing back and forth of quasiparticles. We will use the semiconductor model in Fig. 2 to help to understand both the photon-assisted tunneling and the quantum sloshing. The superconducting energy gap 2Δ splits the density of quasiparticle states into two separate bands, the conduction band and the valence band. At $T=0$, all the states in the valence band are full and all the states in the conduction band are empty. The dc bias voltage V_0 shifts the relative Fermi levels on the two sides by eV_0. Consider a SIS junction in the presence of a photon field with photon energy $\hbar\omega$. Conservation of energy allows transitions to take place only between two states whose energy difference is $\hbar\omega$. Also at $T=0$, Pauli's exclusion principle requires that if one state is in the valence band then the other state must be in the conduction band.

The tunneling between states A and B in Fig. 2, which satisfies the condition $E_A+\hbar\omega=E_B$, is the photon-assisted tunneling[16] which gives rise to a steplike structure on the dc I-V curve of a pumped SIS junction. This

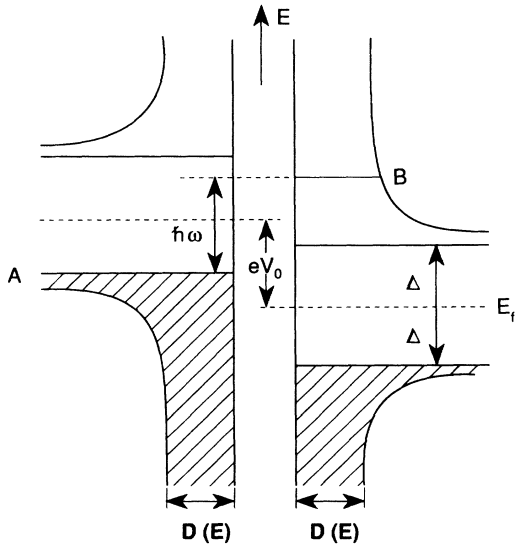

FIG. 2. Semiconductor model of a SIS junction. The energy difference between state A on the left-hand side and state B on the right-hand side is $\hbar\omega$, where ω is the angular frequency of the rf drive. The tunneling between states A and B can be assisted by the photons in the rf signal. The tunneling between state A and any states other than B cannot be completed because of the energy conservation law. The quantum sloshing between state A and states above B gives a capacitive component, while the sloshing between state A and states below B gives an inductive one.

tunneling can also be assisted by absorbing more than one photon if the photon field is strong enough. The tunneling of a quasiparticle in an initial state A to final states other than B cannot occur because it violates conservation of energy. However, this does not imply that the tunneling between two such states can never take place. A quasiparticle in state A can absorb a photon $\hbar\omega$ temporarily to tunnel to a state on the right-hand side other than state B, then emit a photon of the same frequency and tunnel back to state A. This movement has been called "quantum sloshing" and its primary effect is to alter the phase of the photon field and leave the total photon number unchanged.[3] Therefore, the contribution of this quantum sloshing to the quasiparticle tunneling current is the reactive component, which is what we called quantum susceptance. As pointed out by Tucker,[3] this susceptance is a consequence of the noninstantaneous current-voltage relation in the quantum-mechanical tunneling.

The sign of the susceptance contributed by the quantum sloshing between two states with energies E_L and E_R depends on whether the energy difference $|E_R-E_L|$ is larger or smaller than the energy of the photons $\hbar\omega$ of the rf drive. If $|E_R-E_L|>\hbar\omega$, then the susceptance is capacitive, if $|E_R-E_L|<\hbar\omega$, the susceptance is inductive. When the energy difference between the two states is equal to the energy of the photons, the tunneling is purely resistive. These results can be understood if we model the SIS as a superposition of two-level systems.

Consider two quasiparticle states, one on the left-hand side and the other on the right-hand side of a SIS junction whose energy difference is $\hbar\omega_{2-l}$. The transition between these two states is analogous to the transition between two levels in an atom. Following Yariv's derivation,[17] the electrical dipole moment $\mathbf{P}(t)$ induced by such a transition can be characterized by the "atomic" susceptibility $\chi=\chi'=i\chi''$, such that

$$\mathbf{P}(t)=\mathrm{Re}(\epsilon_0\chi\mathbf{E}e^{i\omega t}) ,$$

where $\mathbf{E}$ is the external electrical field. The current associated with this time-varying dipole is the time derivative of the electrical dipole moment,

$$I(t)\propto d\mathbf{P}(t)/dt=\mathrm{Re}(i\omega\epsilon_0\chi\mathbf{E}e^{i\omega t}) .$$

Since the rf voltage V_ω is proportional to the electrical field $\mathbf{E}$, the rf admittance $Y_{2-l}(\omega)$ is proportional to $(i\omega\epsilon_0\chi)$. Here the subscript "$2-l$" is to emphasize that this admittance is the contribution only from the tunneling between these two specific states. Then, from Eqs. (8.1)–(8.19) in Ref. 17, we obtain the expression for the quantum conductance and susceptance which arise from these two states in the absence of inelastic scattering during the tunneling,

$$G_{2-l}(\omega)\propto\omega\chi''\propto\frac{\omega}{1+(\omega-\omega_{2-l})^2\tau^2} , \tag{10a}$$

$$B_{2-l}(\omega)\propto\omega\chi'\propto\frac{\omega(\omega_{2-l}-\omega)\tau}{1+(\omega-\omega_{2-l})^2\tau^2} . \tag{10b}$$

Here τ is the lifetime of the quasiparticle concerned. From Eq. (10b), at $\omega>\omega_{2-l}$, B_{2-l} is negative and the susceptance is inductive, and at $\omega<\omega_{2-l}$, B_{2-l} is positive and the susceptance is capacitive. Finally, at $\omega=\omega_{2-l}$, B_{2-l} is zero and the admittance is purely resistive and the conductance G_{2-l} takes a maximum value. If we assume that the quantum sloshing processes are uncorrelated,[19] the total quantum conductance $G_Q(\omega)$ and the quantum susceptance $B_Q(\omega)$ are computed by integrating G_{2-l} and B_{2-l} over all the quasiparticle tunneling processes allowed by Pauli's principle. These results can also be understood qualitatively from the behavior of a classical harmonic oscillator with an intrinsic frequency ω_{2-l}. When the drive varies slowly with time, $\omega<\omega_{2-l}$, the displacement, which is proportional to the dipole moment, follows the drive, i.e., $\mathbf{P}\propto\mathbf{E}$. When the drive varies rapidly with time, $\omega>\omega_{2-l}$, the displacement is 180° out of phase with the drive, so $\mathbf{P}\propto -E$.

Returning to the formal theory, we plot in Fig. 3 the calculated quantum conductance $G_Q(\omega)$ and the quantum susceptance $B_Q(\omega)$, using Eqs. (5) and (8) and the I_{dc} and I_{KK} in Fig. 1, as functions of frequency at a fixed dc bias voltage $V_0=2.50$ mV. The peak of G_Q at 62 GHz occurs when the photon energy is equal to the energy difference between the edge of the conduction band on one side and the edge of the valence band on the other side of the junction. This frequency is a simple function of dc bias voltage, $f_0=(V_g-V_0)/h$. At this frequency, the quantum susceptance B_Q vanishes just as what we expect for a two-level system. At frequencies below f_0, B_Q is positive and the quantum susceptance is capacitive; at frequencies above f_0, B_Q is negative and the quantum susceptance is inductive. The plot in Fig. 3 is strikingly similar to Fig. 8.2 in Ref. 17, where the real and imaginary parts of the

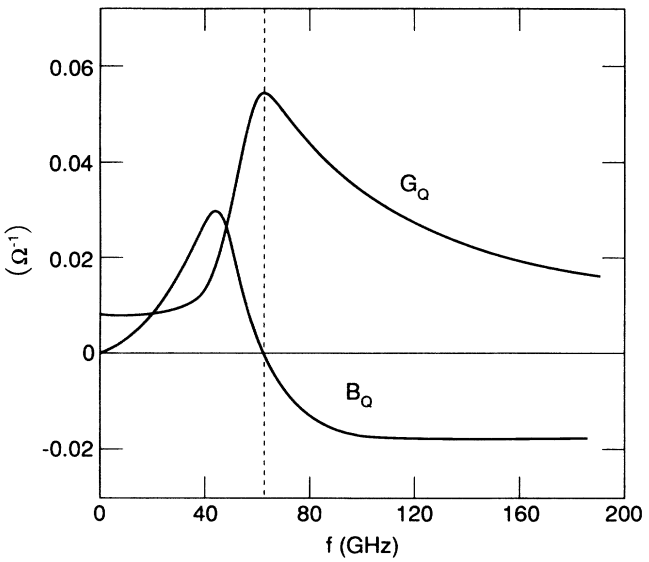

FIG. 3. Quantum conductance G_Q and quantum susceptance B_Q calculated as functions of frequency at a dc bias voltage $V_0=2.50$ mV using Eq. (8). The frequency f_0 at the peak of G_Q, 62 GHz, corresponds to the energy difference between the edges of the valence band and of the conduction band on two sides of the junction, i.e., $f_0=e(V_g-V_0)/h$. At this frequency, the quantum susceptance B_Q vanishes.

atomic susceptibility $\chi' \propto B_{2-l}/\omega$ and $\chi'' \propto G_{2-l}/\omega$ are plotted as functions of frequency. This strong similarity suggests that a SIS junction can be approximated as a voltage-tunable two-level system whose energy difference is $e(V_g - V_0)$. This approximation is valid because of the singularities of the quasiparticle density of states at the gap energy so a large portion of the quasiparticles occupy the states near the gap.

Using the discussion in the last two paragraphs, we can provide a detailed physical explanation of the voltage dependence of the quantum susceptance. At $V_0 < V_g - \hbar\omega/e$, the energy difference between all the states in the conduction band on one side and all the states in the valence band on the other side is greater than the photon energy, i.e., $\omega_{2-l} > \omega$. Therefore, $Y_{2-l}(\omega)$ from all possible quantum sloshing events are capacitive. As V_0 increases from zero to $V_g - \hbar\omega/e$, the difference $(\omega_{2-l} - \omega)$ becomes smaller, so the denominator in Eq. (10b) decreases. This results in a maximum capacitive value of the quantum susceptance B_Q at $V_g - \hbar\omega/e$, as shown in Fig. 1(d). As the bias voltage V_0 increases from $V_g - \hbar\omega/e$, there will be states in the conduction band with energy less than $\hbar\omega$ greater than some of the states in the valence band on the other side. For these pairs of states, $\omega_{2-l} < \omega$, so their contribution to the quantum sloshing is inductive. This explains why the quantum susceptance B_Q becomes more inductive as V_0 increases from $V_g - \hbar\omega/e$, and has the largest inductive value at the gap voltage V_g, as shown in Fig. 1(d).

Although the above discussion was carried out at $T=0$ for simplicity, the results are still valid at finite temperature. Two modifications should be introduced in the above discussion at finite temperatures. First, the superconducting energy gap is reduced. Second, the states in the valence band are not completely filled, the occupation probability is given by the Fermi distribution $f(E)$. Similarly, the states in the conduction band are not completely empty, and the unoccupied probability is given by $1-f(E)$. These two modifications at finite temperature affect the dc I-V curve in the same way as they affect the high-frequency response of the SIS junction. Therefore, the rf admittance of a SIS junction is still given by Eqs. (8a) and (8b) as long as its dc I-V curve at $T \neq 0$ is still due to elastic tunneling.[2]

In the general case, $\alpha = eV_\omega/\hbar\omega$ can be any value and we must consider a complicated nonlinear solution of Eq. (7) to analyze the response of a SIS junction to rf radiation. We can still define an admittance $Y(\omega) = I_\omega/V_\omega$, where I_ω and V_ω are the current and voltage at frequency ω. In this case, $Y(\omega)$ will be a function of V_ω as well as a function of V_0 and ω. Numerical computation is required for detailed analysis. However, some of the qualitative features discussed above in the linear limit will still apply as long as α is not so much greater than unity that multiphoton processes dominate the one-photon process.[12] One of the important features is that the quantum susceptance takes its maximum capacitive value at one-photon voltage below the gap $V_g - \hbar\omega/e$, and changes to an inductive value as the bias voltage increases to the gap voltage V_g. We will show later in Sec. IV that this feature is responsible for the photon-assisted-tunneling steps with negative dynamic resistance which were observed at drive frequencies slightly below the resonant frequency of a microstrip stub resonator.

III. EXPERIMENTAL DETAILS

As discussed in Sec. II, the reactive part of the quasiparticle response function or, equivalently, the quantum susceptance B_Q has no contribution to the tunneling current when the bias voltage is purely dc, i.e., $V(t) = V_0$. Also, the quantum susceptance B_Q has no effect on the dc I-V curve of a SIS junction pumped by a rf voltage source whose amplitude V_ω is independent of dc bias voltage. Consequently, the quantum susceptance cannot be measured in a dc voltage-biased SIS junction, or from the dc I-V curves of a rf voltage-biased SIS junction.

The most straightforward and convenient way to measure a reactive element is to measure the resonant frequency of a resonator which contains the element to be measured. In a less direct way, the quantum susceptance B_Q can be measured from the shape of the I-V curves of a SIS junction pumped by a rf source with a nonzero output impedance. The first method gives a direct and definitive measurement of the quantum susceptance. The second method gives an independent check and can also help in understanding the role of the quantum susceptance in the rf impedance match, especially in the large-signal limit. This impedance match is crucial for many SIS devices, such as SIS direct detectors,[19] SIS heterodyne mixers,[3,4] and SIS parametric amplifiers.[20] We describe both ways of measuring the quantum susceptance in this paper.

We have constructed a millimeter wave resonant circuit by using a superconducting microstrip stub and a SIS junction. This resonator is quasioptically coupled to the radiation source by a planar antenna and several lenses.[21] A photograph and a schematic drawing of the junction and microstrip stub located at the center of a log-periodic antenna are shown in Figs. 4(a) and 4(b). The response of this resonator to a rf signal can be analyzed using the equivalent circuit shown in Fig. 4(c). The signal and the antenna are represented by a rf current source in parallel with its source admittance Y_A. The SIS junction is represented by the parallel combination of the quantum conductance $G_Q(\omega)$, quantum susceptance $B_Q(\omega)$, and the geometric capacitance C. The admittance of the superconducting microstrip stub is essentially reactive and can be represented by a susceptance $B_{\text{stub}}(\omega)$. The loss of the stub at rf can be modeled by a conductance in parallel with $B_{\text{stub}}(\omega)$. This loss does not affect the value of the susceptance $B_{\text{stub}}(\omega)$ to first order, and therefore it is unimportant in the determination of the resonant frequency of the resonator.

In order to measure the quantum susceptance B_Q, we need to know the imbedding susceptance B_{imb}, which is the total susceptance that is independent of dc bias voltage. In the equivalent circuit in Fig. 4(c), the imbedding susceptance B_{imb} is the sum of the susceptances of the junction capacitance ωC, and of the microstrip stub

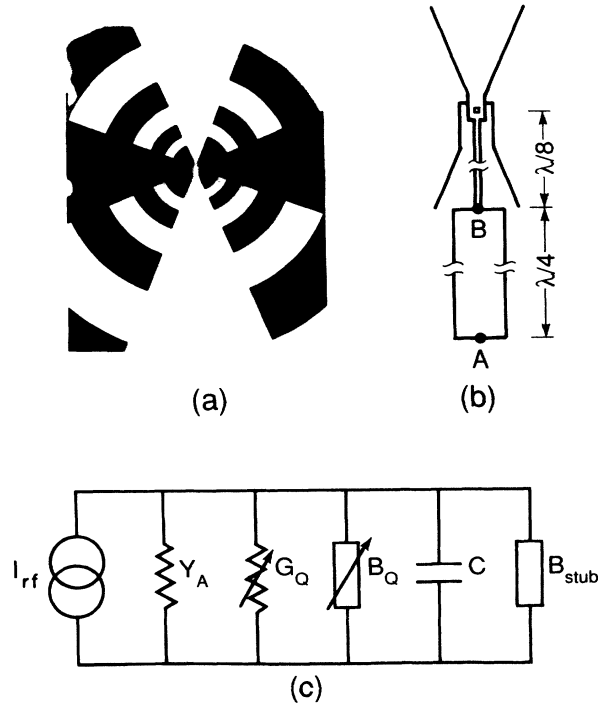

FIG. 4. (a) Picture of a log-periodic antenna with a microstrip stub. The SIS junction is located at the center of the antenna at one end of the stub. (b) Schematic of a two-section microstrip stub. The $\lambda/4$ section which is open circuited at point A produces a short circuit at point B. (c) Equivalent circuit of a resonator which includes a microstrip stub with susceptance B_{stub}, a junction capacitance C, the quantum susceptance B_Q, and the quantum conductance G_Q. The variable signs on B_Q and G_Q indicate that they are functions of dc bias voltage. The radiation source and the antenna are represented with a rf current source in parallel with the antenna admittance Y_A.

$B_{\text{stub}}(\omega)$, and of the antenna $\text{Im}(Y_A)$. The resonance of the equivalent circuit of Fig. 4(c) corresponds to the condition

$$B_{\text{tot}}=B_Q(\omega)+B_{\text{imb}}(\omega)=0 .$$

Without the quantum susceptance B_Q, the resonant frequency would be independent of bias voltage. However, since B_Q changes rapidly with dc bias voltage V_0 as shown in Fig. 1(d), we expect that the resonant frequency will change as V_0 changes.

The susceptance of the capacitance is simply ωC, and the susceptance of the stub $B_{\text{stub}}(\omega)$ can be calculated using formulas in a standard microwave engineering textbook.[22] The expression of the susceptance of an antenna can be quite complicated in general. However, for a special class of planar antennas called "self-complementary antennas," in which the pattern of the metallic part is the same as that of the dielectric part, the admittance of the antenna is real and independent of frequency.[23] The antenna admittance is given by

$$Y_A=(1+\epsilon_r)^{1/2}3.74\times10^{-1}\Omega^{-1} ,$$

where ϵ_r is the relative dielectric constant of the substrate. Use of a self-complementary antenna greatly simplifies the characterization of the imbedding admittance. In this experiment, we have used a circular-toothed log-periodic antenna which was measured to have a high antenna efficiency ($\sim$60%) and a nearly Gaussian antenna beam pattern.[24] As shown in Fig. 4(a), the antenna is self-complementary. We have used a fused quartz substrate, which has a relative dielectric constant $\epsilon_r=3.85$ at millimeter wave frequencies.[25] This gives an antenna admittance of $Y_A=8.3\times10^{-3}\Omega^{-1}$.

We have used a superconducting microstrip stub with the stub made out of Pb-In-Au alloy and the ground plane of Nb. As shown in Figs. 4(a) and 4(b), the stub contains two sections, a narrow section 1 and a wide section 2. The widths and the lengths of the two sections are $w_1=6$ μm, $w_2=40$ μm, $l_1=135$ μm, and $l_2=260$ μm. The phase velocity within the microstrip line is $v=1(L_sC_s)^{1/2}$, where

$$L_s=(\mu_0/kw)[t+\lambda_1\coth(t_1/\lambda_1)+\lambda_2\coth(t_2/\lambda_2)]$$

is the inductance per unit length,[26] and $C_s=k\epsilon_r\epsilon_0 w/t$ is the capacitance per unit length.[26] t and ϵ_r are the thickness and the dielectric constant of the insulating layer (SiO in our case), $t_{1,2}$ and $\lambda_{1,2}$ are the thicknesses and the London penetration depth of the ground (Nb) and top (Pb-In-Au) plane, and k is a fringing factor close to unity. Using the designed values, $\epsilon_r=5.7$,[27] $t=3000$ Å, $t_1=2000$ Å, $t_2=4250$ Å, $\lambda_{\text{Nb}}=850$ Å,[27] $\lambda_{\text{Pb-In-Au}}=1450$ Å,[27] the phase velocity is $v=(0.30\pm0.01)c$. The length of the wider section is $\frac{1}{4}$ of the wavelength at 87 GHz, so the wider section transforms a rf open circuit at point A to a rf short circuit at point B in Fig. 4(b).[22] This two-section stub has a slower variation of the susceptance as a function of frequency than a one-section open-ended stub, so the effect of the quantum susceptance is more profound.[28] The length of the narrow section is $\frac{1}{8}$ of the wavelength at 85 GHz which transforms the rf short to an inductive admittance. The total susceptance of the two-section stub is given by[22]

$$B_{\text{stub}}(\omega)=\frac{Y_1[Y_2\tan(\beta l_2)+Y_1\tan(\beta l_1)]}{Y_1-Y_2\tan(\beta l_1)\tan(\beta l_2)} , \qquad (11)$$

where $\beta=\omega/v$, $Y_{1,2}=(C_{s1,2}/L_{s1,2})^{1/2}$ are the characteristic admittances of section 1 (narrow) and section 2 (wide) of the stub, $Y_1=0.124\Omega^{-1}$, and $Y_2=0.637\Omega^{-1}$. We have shown that the expression of the susceptance of the stub $B_{\text{stub}}(\omega)$ remains the same when there is a small rf loss in the stub.[29]

In order to measure the small-signal frequency response of the junction-stub resonator, the rf power coupled to the resonator must be less than 10 pW so, for $G_Q=0.01\Omega^{-1}$, $\alpha=eV_\omega/\hbar\omega\ll1$ at 75 GHz and Eq. (8) applies. Consequently, we need a very sensitive detector. Also, the frequency dependence of the detector must be known in order to separate the frequency response of the resonator from that of the detector. We have used the internal detection mechanism in the SIS junction to measure the frequency response of the resonator. SIS direct

detectors are known to be among the most sensitive 4.2-K video detectors at millimeter wave frequencies,[30] and they have been proved to be very useful in measuring the frequency response of millimeter and submillimeter wave resonators.[29] The frequency-dependent responsivity of the SIS direct detector can be easily calculated from Tucker's theory.[3] There is also a major advantage of this scheme: because of the proximity of the SIS detector to the resonator, there is no Fabry-Perot interference between them. The output of the SIS detector as a function of rf is the product of the frequency response of the resonator, the spectrum of the source, and the frequency-dependent responsivity of the SIS detector.

The current responsivity S_I of a SIS direct detector, defined as the induced dc current per unit rf power absorbed, as a function of frequency is given by[3]

$$S_I(\omega)=\frac{\Delta I_{\rm dc}}{P_\omega}=\frac{e}{\hbar\omega}\frac{I_{\rm dc}(V_0+\hbar\omega/e)-2I_{\rm dc}(V_0)+I_{\rm dc}(V_0-\hbar\omega/e)}{I_{\rm dc}(V_0+\hbar\omega/e)-I_{\rm dc}(V_0-\hbar\omega/e)} . \tag{12}$$

Here $P_\omega=\mathrm{Re}(I_\omega V_\omega^*/2)$ is the rf power actually dissipated in the SIS junction. Note the absence of the reactive quasiparticle response function $I_{\rm KK}$ in Eq. (12), which implies that the quantum susceptance B_Q does not affect the responsivity. As pointed out by Tucker,[3] $S_I(\omega)$ reduces to a frequency-independent classical current responsivity $(d^2I/dV^2)/2(dI/dV)$ at low frequencies, and approaches a quantum limit $e/\hbar\omega$ at frequencies so high that the voltage associated with one photon $\hbar\omega/e$ is larger than the width of the current rise at the sum gap voltage. The induced dc current per unit available rf power P_A in the SIS junction as a function of rf is then given by

$$\frac{\Delta I_{\rm dc}}{P_A}=S_I(\omega)\left[1-\left|\frac{Y_A-Y_J^*}{Y_A+Y_J}\right|^2\right], \tag{13}$$

where $Y_J=G_Q+i(B_Q+\omega C+B_{\rm stub})$ is the total admittance of the SIS junction and the stub, and $S_I(\omega)$ is the current responsivity defined in Eq. (12). The second factor on the right-hand side of Eq. (13) is the rf coupling coefficient $C_{\rm rf}$ defined in previous publications.[21] $C_{\rm rf}$ is the fraction of the available rf power which is delivered to the dissipative element G_Q. Equation (13) implies that the induced dc current is the product of the rf coupling coefficient $C_{\rm rf}(\omega)$ and the current responsivity $S_I(\omega)$. Since $S_I(\omega)$ is a smooth function of frequency except at $e(V_g-V_0)/\hbar$, the frequency dependence of the rf-induced dc current $\Delta I_{\rm dc}$ is mainly determined by the frequency dependence of $C_{\rm rf}(\omega)$. Therefore, the frequency which corresponds to the maximum $\Delta I_{\rm dc}$ is mainly determined by the resonance condition of the resonator; that is,

$$\mathrm{Im}(Y_J)=B_Q+\omega C+B_{\rm stub}=0 .$$

When this condition is met, the rf coupling coefficient $C_{\rm rf}$ has the maximum value.

We also need to know the power spectrum of the rf source. We have used both a tunable coherent millimeter wave source which utilizes the Gunn effect[31] and an incoherent source from the output of a Fourier-transform spectrometer (FTS). Calibration of the coherent power incident upon the resonator was difficult due to Fabry-Perot resonance within the source. These resonances have sharper peaks than that of the stub-junction resonator so they dominated the measured response. The short coherent length of the radiation from the FTS eliminates most of this problem. In this paper, the resonant frequencies and the widths of the resonances of the stub-junction resonator were measured using the FTS. The coherent source was used to study the shape of the photon-assisted-tunneling I-V curves.

The FTS used in this experiment is a far-infrared Michelson interferometer[32] operated in the step-and-integrate mode. The output spectrum of the FTS is the blackbody radiation from a Hg arc lamp at 500 C°, modified by the efficiency of a 250-μm-thick Mylar beamsplitter. Since the antenna-coupled SIS direct detector is sensitive to only a single electromagnetic mode, and the source is in the Rayleigh-Jeans limit, the power spectrum of the source is given by a constant multiplied by the beamsplitter efficiency $\eta_{\rm bm}$, which is a smooth function of frequency.[29] For 250-μm-thick Mylar film at 45° to the beam with a relative dielectric constant $\epsilon_r=3$, the beamsplitter efficiency $\eta_{\rm bm}$ is slowly increasing with frequency in the frequency range of interest.[29]

The experimental apparatus used in this work is essentially the same as was used in our quasioptical SIS mixer experiment.[21] The output of the FTS is connected to the cryostat through a 1-m-long, 11-mm-diam light pipe. The cryostat has a 25-mm-diam window which is covered with a 25-μm-thick polypropylene window, which should transmit almost 100% at millimeter wave frequencies. Within the cryostat, the signal beam is focused by a $f/0.85$ TPX lens, and then further focused by a hyperhemispherical quartz lens to a $f/0.5$ converging beam whose beam waist occurs at the flat side of the hyperhemispherical quartz lens, where the log-periodic antenna with the junction and the resonator is centered. The quartz lens is heat sunk to the liquid-helium tank through a copper support. The temperature of the SIS junction is estimated to be 4.5 K for an unpumped helium bath. Under unpumped conditions, the liquid helium in the cooling tank can last about 10 h as compared to ~5 h when the helium is pumped. The longer hold time allows us to improve the signal-noise ratio by using longer integration times. Therefore, all the results reported in this

paper were obtained at 4.2-K bath temperature. This temperature is cold enough for our experiment since our all-Nb SIS junctions have a relatively high T_c ($\sim$9 K) so the operating temperature is about half of the transition temperature.

The SIS junction used in this experiment was fabricated at the National Institute of Standards and Technology at Boulder. It is a Nb/Al_2O_3/Nb sandwich made using the trilayer process.[33] The critical current density of the SIS junction is about 500 A/cm^2. The normal resistance of 70Ω is approximately matched to the antenna impedance. The I-V curve of the junction shows a low-leakage current and a sharp gas structure even at 4.5 K, as shown in Fig. 1(a). The sharp gap structure causes a dramatic peak in $I_{KK}(V)$ at the gap voltage V_g. This peak, and the associated large values of curvature, are essential to observe the effects of the quantum susceptance as discussed above. The junction has been thermally cycled between room temperature and liquid-helium temperature over 30 times, and the I-V characteristic has not changed. The junction area is estimated to be 2.5×2.5 μm^2, which gives a geometric capacitance of 0.28 ± 0.03 pF if we assume a specific capacitance value of 45 ± 5 fF/μm^2.[34] This capacitance value gives a susceptance of $0.14\Omega^{-1}$ at 80 GHz. Figure 1(d) indicates that the change of the quantum susceptance is as large as $0.05\Omega^{-1}$ between 2.4 and 2.7 mV, which is significant compared to that of the junction capacitance. Therefore, the change of the quantum susceptance as a function of dc bias voltage should have a very noticeable effect on the resonant frequency of the stub-junction resonator.

IV. DATA ANALYSIS

In this section we will discuss the procedures for measurement and the comparison between the experimental data and the theoretical calculations. Two types of data will be presented: One is the measured resonant frequency and the width of the resonance peaks as functions of dc bias voltage. These data were obtained from spectra measured in the small-signal limit using a Fourier-transform spectrometer. The other is the I-V curves pumped by a coherent rf signal with sufficient power that photon-assisted-tunneling steps are clearly seen. The frequencies of the rf pump is close to the resonant frequency of the imbedding admittance so the effect of the quantum susceptance is significant in affecting the shape of the I-V curves. In both types of data, the quantum susceptance proved easily measurable.

A. Frequencies and widths of the resonance peaks

The interferograms in this experiment were obtained from the rf-induced dc current ΔI_{dc} as defined in Eq. (13) as a function of the difference between the two optical paths of the FTS. These interferograms were measured in the step-and-integrate mode, with the integration time typically $\sim$1.5 sec. The spectra were obtained by Fourier transformation of the product of the interferogram and the apodization function.[35] We chose to use an apodization function with a form of $[1+\cos(x\pi/x_{max})]/2$, where x is the path length difference and x_{max} is the maximum of the path length difference used in the experiment. This apodization function lowers side peaks of the spectrum at the expense of a moderate increase of the width of the resonance peak. Figures 5(a) and 5(b) show interferograms taken at two bias voltages, $V_0=2.350$ and 2.500 mV. At $V_0=2.350$ mV, the value of the quantum conductance G_Q is low as shown in Fig. 1(c), so the Q value of the stub-junction resonator is high and the peak of the resonance is narrow. Consequently, the fringe amplitude decreases slowly as the path difference increases as shown in the interferogram in Fig. 5(a). At $V_0=2.500$ mV, the value of the quantum conductance G_Q is high due to the onset of the photon-assisted tunneling, so the Q value of the stub-junction resonator is low and the peak of the resonance is broader than that measured at $V_0=2.350$ mV. Consequently, the fringe visibility in the interferogram decreases rapidly as the path difference increases as shown in Fig. 5(b). The corresponding spectrum shown in Fig. 5(d) shows a broader peak than that in Fig. 5(c). Besides the apparent difference in the widths of the resonances in the two spectra, the frequencies which correspond to the peaks of the two spectra differ by a noticeable amount.

In order to improve the signal-noise ratio of the measured spectra, we have co-added 5–10 spectra measured at a given bias voltage. After normalizing these spectra to the beamsplitter efficiency η_{bm}, we obtain the resonant frequencies by least-mean-squares fitting the top 50% part of the resonance peaks with second- to fourth-order polynomials. The degree of the polynomials in the fitting is determined by the asymmetry of the peak. The error bars on the measured resonant frequencies are chosen as the frequency ranges in which the fitting polynomials are over 90% of their peak values. The result is plotted in Fig. 6(a) as a function of dc bias voltage V_0. Below 2.150 mV and above 2.650 mV, the signal-noise ratio of the spectra is very poor due to the rolloff of the current responsivity S_I of the SIS direct detector. Therefore, no data are plotted outside of this range. The error bars are twice as large for $V_0\geq2.450$ mV as those for <2.450 mV

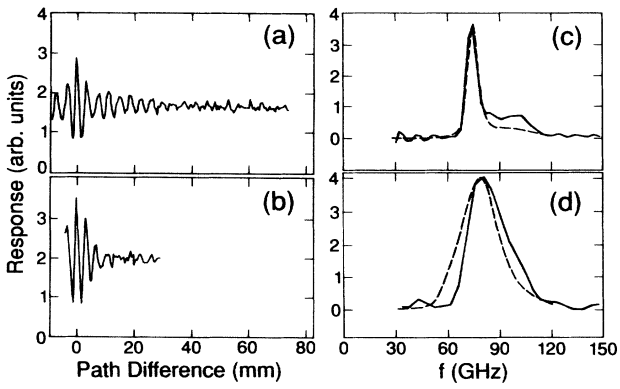

FIG. 5. Interferograms measured with a Fourier-transform spectrometer (a) at 2.35 mV and (b) at 2.50 mV. Spectra after correcting for beamsplitter efficiency corresponding to the above interferograms (c) at 2.35 mV and (d) at 2.50 mV. The dashed lines in (c) and (d) are the computed spectra.

because the peaks are broader for $V_0 \geq 2.450$ mV due to the sharp increase of the quantum conductance G_Q. Fabry-Perot fringes appear on these broad peaks if we keep the resolution of the FTS the same as for the narrow peaks. These Fabry-Perot fringes probably arise from the standing waves between the SIS junction and the TPX lens. In order to average over those Fabry-Perot fringes, we have used a lower resolution of 0.3175 cm^{-1} in our FTS which resulted in large error bars for the measured resonant frequencies above 2.450 mV. The experimentally measured resonant frequencies clearly show a smooth shift as the dc bias voltage changes. The most dramatic change of the resonant frequency takes place within the voltage range from 2.400 to 2.650 mV, it changes from 73 to 87 GHz. From Fig. 1(d), we can see that the quantum susceptance B_Q changes rapidly from capacitive to inductive in exactly the same voltage range.

In order to make accurate comparisons between theory and experiment, we obtain the theoretically calculated resonant frequencies using the same method used to obtain the experimental resonant frequencies. First, we compute the rf-induced dc current as a function of rf using Eq. (13). Second, we convolve these computed spectra with the Fourier transform of the apodization function which was used in the Fourier transformation of the experimental interferograms.[35] Third, we chose the same number of computed data points at the same discrete frequencies as we did from the experimental data. Finally, for each spectrum, we fit these discrete computed points with a polynomial with the same degree as was used in fitting the experimental data. The theoretically calculated curve for the resonant frequency as a function of V_0 is shown in Fig. 6(a) as the solid line, and it is in excellent agreement with the experimental results. We would like to emphasize that the values of two key parameters, the junction capacitance $C=0.275$ pF and the phase velocity $v=0.286c$, which were used in our theoretical computation, are essentially the same as the ones we estimate from the geometric dimensions 0.28 ± 0.03 pF and $(0.30\pm0.01)c$. As a comparison, the dashed line, which is essentially flat and obviously differs from the experimental results, is the theoretically calculated resonant frequency as a function of V_0 without including the quantum susceptance B_Q. The weak voltage dependence of the dashed line is due to the change of the current responsivity $S_I(\omega)$ with V_0. Clearly, these results provide decisive evidence for the quantum susceptance.

We have also investigated the effect of Josephson oscillation on the shift of the resonant frequency by applying a magnetic field to change the Josephson critical current. From Eqs. (1) and (2), we can see that the pair tunneling current also contains a reactive component, the $\sin\phi$ term. This reactive component from the pair tunneling may also affect the resonant frequency of the stub-junction resonator. If there is any significant effect from the pair tunneling, then this effect should be changed as we modulate the Josephson critical current with a magnetic field. We did not measure any change of the resonant frequency within our experimental accuracy up to a field corresponding to several quanta of magnetic flux in the SIS junction. This is probably because, at bias voltages from 2.15 to 2.65 mV, the Josephson current oscillates at frequencies above 1 THz, which is completely shunted by the junction capacitance.

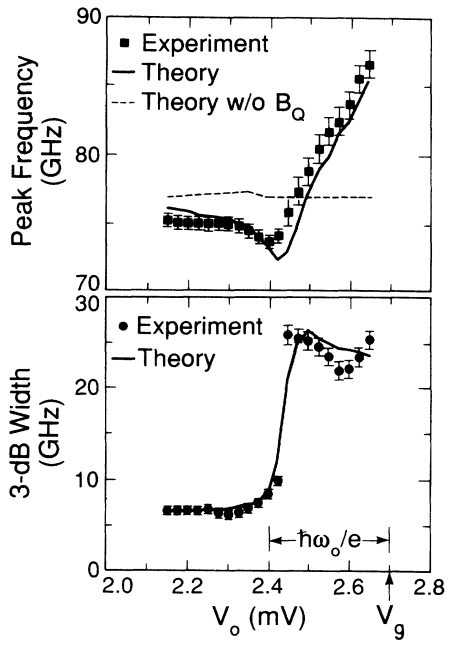

FIG. 6. (a) Resonant frequency as a function of dc bias voltage. The solid circles are the experimentally measured results, the sold line is theoretically calculated, the dashed line is the calculated result without including the quantum susceptance. Note the dashed line is essentially flat vs V_0. (b) Linewidth of the resonance as a function of V_0. The solid circles are the experimental results and the solid line is the calculated result. The resonant frequency of the imbedding susceptance without the quantum susceptance is $\omega_0/2\pi=77$ GHz.

We discovered a strong signal at the output of the SIS detector at $V_0=0.158$ mV, which corresponds to a 77-GHz Josephson oscillation. The level of this strong signal is comparable to the largest signal obtained in the voltage range from 2.100 to 2.650 mV using quasiparticle direct detection. This detection is a result of a Josephson homodyne detection in a self-pumped mode. In this mode, the Josephson current, which oscillates at $\omega_j/2\pi=2eV_0/h=77$ GHz, and which coincides with the resonant frequency of the microstrip stub resonator, mixes with the rf signal at the same frequency and produces a dc output. We found that the signal level at the output of the detector is a very sensitive function of the dc bias voltage. At voltages below 0.150 mV and above 0.170 mV, the signal level decreases to essentially the level of the broadband noise. Similar detection mode was reported by Richards and Sterling,[36] in which the Josephson detector exhibited a very narrow frequency response at the resonant frequency of a cavity. The interferogram obtained in this detection mode is very similar to those obtained using quasiparticle direct detection. The peak frequency of the resonance is the same as the Josephson oscillation frequency, 77 GHz. We would like to point out at this low bias voltage, the curvature of $I_{KK}(V)$ is al-

most zero, as can be seen from Fig. 1(b). So the quantum susceptance is negligible compared to that of the imbedding structures. In addition, the susceptance of the Josephson $\sin\phi$ term is negligible at this low rf power level.[8] Therefore, the measured resonant frequency should be the resonant frequency of the microstrip stub and the junction capacitance. The coincidence of this measured resonant frequency and the calculated one without including the quantum susceptance [dashed line in Fig. 6(a)] is an additional verification of the values of the junction capacitance C and the phase velocity v which are used in our calculations.

In Fig. 6(b), we plot the 3-dB linewidths Δf of the resonance peaks as a function of the dc bias voltage. The experimental value of Δf were obtained from the best-fitted polynomials. The solid line is calculated using the same apodization function used in the experiment. Again, the agreement between experiment and theory is excellent. This comparison provides an additional verification of the values of C and v in our calculations. The sharp increase of Δf at 2.450 mV corresponds to the sharp increase of the quantum conductance G_Q at one-photon voltage $\hbar\omega/e$ below the gap voltage V_g. Note from Fig. 1(d) that the quantum susceptance has the largest capacitive value at this voltage, $V_g-\hbar\omega/e$, so the resonant frequency is the lowest as shown in Fig. 6(a). There is some disagreement between the theoretical and experimental values of Δf at $V_0 \geq 2.45$ mV. This discrepancy arises because the quantum conductance G_Q depends on the I-V curve around $V_0+\hbar\omega/e$ which, at $V_0 \geq 2.45$ mV, lies just above the sum gap voltage. Our junction exhibits a negative resistance in this region due to this proximity effect.[37] This is not correctly measured by our I-V curve measurement system. The effect of the proximity effect on the high-frequency response of a SIS junction is currently under investigation.

B. I-V curves of the rf-pumped junction

Photon-assisted-tunneling steps appear on I-V curves of a pumped SIS junction. We will focus on the first step below the gap voltage because this is the voltage region where a SIS heterodyne mixer is usually biased. Also, the quantum susceptance has a significant effect on the dynamic conductance of this step when the rf is close to the resonant frequency of the imbedding admittance.[12] Here we will provide an explanation of how the quantum susceptance affects the dynamic conductance.

Following Smith and Richards,[38] the dynamic conductance can be divided into two parts,

$$G_D=\frac{dI_{\rm dc}(V_0,V_\omega)}{dV_0}$$
$$=\sum_{n=-\infty}^{\infty} J_n^2(\alpha)\frac{\partial I_{\rm dc}(V_0+n\hbar\omega/e)}{\partial V_0}$$
$$+\frac{d\alpha}{dV_0}\frac{\partial}{\partial\alpha}\sum_{n=-\infty}^{\infty} J_n^2(\alpha)I_{\rm dc}(V_0+n\hbar\omega/e)\,, \qquad (14)$$

where $I_{\rm dc}(V_0,V_\omega)$ is the dc I-V curve of a pumped SIS junction defined in Eqs. (6) and (7), $I_{\rm dc}(V_0+n\hbar\omega/e)$ is the dc I-V curve of an unpumped SIS junction evaluated at a bias voltage $V_0+n\hbar\omega/e$, $\alpha=eV_\omega/\hbar\omega$ is the dimensionless rf voltage.

The first part of Eq. (14) is simply the dynamic conductance of the rf voltage-pumped I-V curve. This is almost always positive except at near the gap voltage for a junction with a pronounced proximity-effect-induced supergap structure.[37] We will ignore this case. The second part is due to the change in rf pump voltage with dc bias voltage. It can be either positive or negative depending on the bias conditions and the imbedding admittance. In order for steps of negative dynamic conductance to occur, this second term must be negative and with an amplitude larger than the first one. We have measured about 40 SIS junctions with millimeter wave stub resonators which show negative steps at frequencies slightly below the resonant frequencies of the imbedding admittance. The resonant frequency ranges from 70 to 270 GHz.[21] We have shown that, for junctions with moderately sharp gap structures, this is primarily due to the change of the quantum susceptance as the dc bias voltage V_0 is changed.[12] It is this systematic and consistent behavior that first drew our attention to the possible effect of the quantum susceptance on the high-frequency response of SIS junctions.

The equivalent circuit in Fig. 4 can still be used to analyze the response of a SIS junction to a rf signal with a large amplitude ($\alpha\approx 1$). However, the quantum conductance G_Q and the quantum susceptance B_Q cannot be expressed in a simple form such as that in Eq. (8). They are now dependent upon the rf pump voltage V_ω and must be evaluated self-consistently at each dc bias point. Values of V_ω can be obtained by using V_ω as a fitting parameter in Eqs. (6) and (7) to calculate the dc current of a pumped junction at a particular dc bias voltage V_0. The induced-rf current I_ω at frequency ω can then be calculated from Eqs. (6) and (7). G_Q and B_Q can be calculated from the real and imaginary parts of the ratio I_ω/V_ω.

Two different imbedding admittances are used to illustrate general trends. One imbedding admittance $Y_{\rm imb}=13.5-j\,6.0\ {\rm m}\Omega^{-1}$, is the estimated imbedding admittance which includes the antenna, junction capacitance, and the stub at 73 GHz. This frequency is 4 GHz below the resonant frequency $f_0=77$ GHz at which the imbedding susceptance is zero. The other imbedding admittance, $Y_{\rm imb}=8.0+j\,40\ {\rm m}\Omega^{-1}$, is the calculated imbedding admittance at 83 GHz, which is at 6 GHz above f_0. Notice that, in Figs. 7(c)–7(f), the shapes of the curves of the quantum conductance and the quantum susceptance for both cases are similar to those in small-signal limit, as shown in Figs. 1(c) and 1(d). The quantum conductance is relatively constant on a step, but changes rapidly between steps. The quantum susceptance, however, changes rapidly on the first subgap and supergap steps. It is this change that is responsible for the rapid change of the rf pump voltage across the first step as shown in Figs. 7(g) and 7(h). When the imbedding admittance is inductive, $Y_{\rm imb}=13.5-j\,6.0\ {\rm m}\Omega^{-1}$, the rf driving voltage is larger at a lower dc bias voltage where the quantum susceptance is capacitive, and smaller at

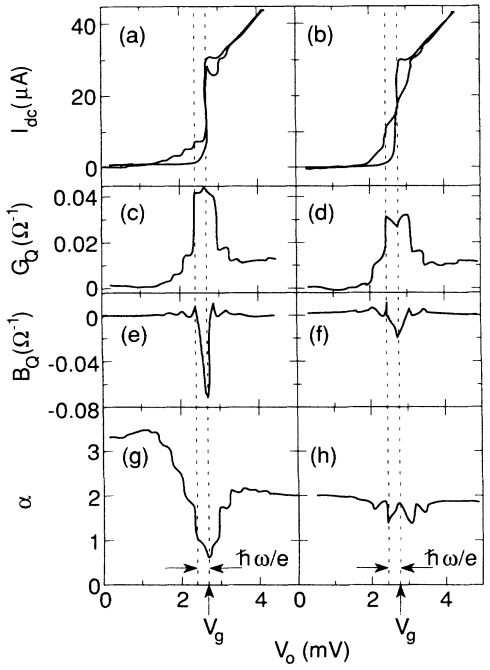

FIG. 7. (a) and (b), dc and pumped *I-V* curves. (c) and (d), quantum conductance G_Q. (e) and (f), quantum susceptance B_Q. (g) and (h), dimensionless rf pump voltage $\alpha = eV_\omega/\hbar\omega$. All quantities are shown with two different imbedding admittances. One, $13.5-j\,6.0$ mΩ^{-1}, is the estimated value at 4 GHz below the $f_0 = 77$-GHz resonant frequency of the imbedding admittance; the other one, $8+j\,40$ mΩ^{-1}, is the estimated value at 6 GHz above f_0. The available rf power is 2.48 nW for (a), (c), (e), and (g), and 17.6 nW for (b), (d), (f), and (h).

higher bias voltage where the quantum susceptance is inductive. Conversely, when the imbedding admittance is capacitive, $Y_{imb} = 8.0+j\,40$ mΩ^{-1}, the rf drive voltage is smaller at lower dc bias voltage than at higher bias voltage. The large negative values of $d\alpha/dV_0$ in Fig. 7(g), caused by the effect of the quantum susceptance on the rf drive voltage, is responsible for the negative photon-assisted-tunneling steps observed in most of our experiments.

Keeping the available rf pump power P_A constant as the dc bias voltage is changed, we compute *I-V* curves for two values of imbedding admittance. At $13.5-j\,6.0$ mΩ^{-1}, the higher photon-assisted-tunneling current at lower bias voltage forms a step with a negative slope. At $8+j40$ mΩ^{-1}, the capacitive quantum susceptance at lower bias voltage lowers the rf drive voltage, resulting in a more positively tilted step. The agreement between these computed *I-V* curves and the measured ones at the same frequencies are essentially perfect as shown in Figs. 7(a) and 7(b). We have also computed *I-V* curves without including the quantum susceptance B_Q. The slope of the first step is quite different from that of the measured *I-V* curve, especially for the one with an inductive imbedding admittance. Negative steps are obtained from the computation which does not include B_Q only for an unrealistically small value of imbedding conductance of $0.001\Omega^{-1}$, which is $\sim 10\%$ of our estimated value. Even using such a small imbedding conductance, only the negative conductance appeared at the extreme low bias voltage end of the first subgap step, in a region that is actually between the first and the second steps. We have never experimentally observed negative dynamic conductance in this region.

We therefore conclude that the quantum susceptance is essential in the production of steps of low or negative dynamic conductance in junctions with moderately sharp sumgap current rises. The frequency region where the negative steps occur is slightly below the resonant frequency f_0 of the imbedding admittance so the imbedding admittance is inductive. This result provides a very effective way to identify whether the imbedding susceptance B_{imb} is inductive or capacitive based on the shape of the photon-assisted-tunneling steps. Since the optimum imbedding susceptance for a double-side-band SIS mixer is usually $B_{imb}=0$,[4,30] this method has proved very useful in searching for the optimum frequencies of SIS mixers coupled to tuning elements.[21]

In order to obtain an excellent fit between the theoretical and the experimental results, we need to use a value of the imbedding conductance of 12.0 mΩ^{-1} at 73 GHz. This value is about 45% larger than that of the log-periodic antenna on a quartz substrate. We suspect that this extra imbedding conductance arises from the microstrip stub which becomes lossy at millimeter wave frequencies. This loss can come either from the surface impedance of the superconducting film or from the dielectric insulating layer. When we cool the SIS junction from ~ 4.5 to ~ 2.5 K, the amount of the extra imbedding conductance remains roughly unchanged. This suggests that the loss does not come primarily from the superconducting films since their loss should decrease rapidly as the temperature is decreased.[39] The loss in the dielectric layer, which is a 3000-Å amorphous SiO layer deposited by thermal evaporation, can be significant at millimeter wavelengths. Empirically, we can model this loss by introducing a parameter γ which characterizes the rf loss per unit length. For small losses $\gamma l \ll 1$, where l is the total length of the stub, the susceptance of the microstrip stub is still given by Eq. (11).[29] Therefore, the above analysis of the quantum susceptance based on the model of a lossless stub is still valid. The conductance of the lossy microstrip stub, however, is nonzero at frequencies below f_0.[29] Since the frequency dependence of γ is unknown, we deduce the actual imbedding admittances by fitting the theoretically calculated *I-V* curves to the experimental ones.

V. CONCLUSIONS

Quantum-mechanical tunneling usually results in a noninstantaneous current-voltage relation if the time scale of the modulation is shorter than the lifetime of the quasiparticles involved. This noninstantaneous current-voltage relation will consequently give rise to a nondissipative reactive component as well as a dissipative, resistive component in the tunneling current. Such a reactive component, which is called the quantum susceptance, should exist in many types of tunneling devices. In a spe-

cial case in which the tunneling is elastic so the quasiparticles emitted from one side of a junction reach the other side at the same energy level, the high-frequency response function can be simply measured from the dc I-V curve. SIS tunnel junctions with high-quality tunnel barriers are one of the examples. Other devices, such as quantum well resonant tunneling devices[40] in which electrons tunnel through a double-barrier quantum well, may also exhibit similar behavior.

The effect of the quantum susceptance is usually complicated at low frequencies because the experimentally acceptable signal-noise ratio requires that the dimensionless rf voltage $\alpha = eV_\omega/\hbar\omega \gg 1$. In this limit, multiphoton processes dominate so the system is highly nonlinear. In a linear scheme in which $\alpha \ll 1$, the effect of the quantum susceptance can be predicted analytically. However, $\alpha \ll 1$ requires sufficiently high frequency so V_ω is large enough for an acceptable signal-noise ratio. We have obtained definitive experimental evidence for the existence of the quantum susceptance by studying the response of a SIS junction to a weak rf radiation at millimeter wavelengths. We have measured the shift of the resonant frequency of a resonator which contains a SIS junction. The observed 19% shift, from 73 to 87 GHz as the dc bias voltage is changed from 2.40 to 2.65 mV, is due to the change of the quantum susceptance with bias voltage. This is in excellent agreement with Werthamer-Tucker theory and is a direct experimental evidence of the existence of the quantum susceptance. Our result has therefore, for the first time, directly verified one of the important aspects of this theory. We have also studied the effect of the quantum susceptance in the large-signal limit by studying the photon-assisted-tunneling steps with negative conductance. This negative conductance is due to the larger rf drive voltage caused by the capacitive quantum susceptance at lower bias voltage. The agreement between the I-V curves calculated including the quantum susceptance and the experimental ones is essentially perfect. This result provides an effective way to identify whether the imbedding admittance is inductive or capacitive by observing the slope of the photon-assisted-tunneling steps. This method has proved to be very useful in searching the optimum frequencies for SIS mixers coupled to tuning elements.

ACKNOWLEDGMENTS

We would like to thank D. Miller and W. N. Creager for assisting the FTS experiment, and J. E. Carlstrom for lending us a 60–90-GHz Gunn oscillator. We would also like to thank M. J. Feldman, M. J. Wengler, and S. Feng for helpful discussions. This work was supported in part by the Director, Office of Energy Research, Office of Basic Energy Sciences, Materials Sciences Division of the U. S. Department of Energy under Contract No. DE-AC03-76-SF00098, and by the Department of Defense.

---

*Present address: Department of Electrical Engineering and Computer Science and Research Laboratory of Electronics, Massachusetts Institute of Technology, Cambridge, Massachusetts 02139.

†Present address: Department of Electrical Engineering, University of Virginia, Charlottesville, Virginia 22901.

[1]N. R. Werthamer, Phys. Rev. **147**, 255 (1966).

[2]R. E. Harris, Phys. Rev. B **10**, 84 (1973); **11**, 3329 (1975); **13**, 3818 (1976).

[3]J. R. Tucker, IEEE J. Quantum Electron. **QE-15**, 1234 (1979).

[4]J. R. Tucker and M. J. Feldman, Rev. Mod. Phys. **57**, 1055 (1985).

[5]J. D. Jackson, *Classical Electrodynamics*, 2nd ed. (Wiley, New York, 1975), Chap. 7.

[6]B. D. Josephson, Phys. Lett. **1**, 251 (1961); Rev. Mod. Phys. **36**, 216 (1964).

[7]A. Barone and G. Paterno, *Physics and Applications of the Josephson Effect* (Wiley, New York, 1982).

[8]K. K. Likharev, *Dynamics of Josephson Junctions and Circuits* (Gordon and Breach, New York, 1986).

[9]H. C. Torey and C. A. Whitmer, *Crystal Rectifiers*, Vol. 15 of *MIT Radiation Laboratory Series* (McGraw-Hill, New York, 1948).

[10]M. J. Feldman, J. Appl. Phys. **53**, 584 (1982).

[11]See, for example, O. H. Soerensen, J. Mygind, and N. F. Pedersen, Phys. Rev. Lett. **39**, 1019 (1977), and references therein.

[12]C. A. Mears, Q. Hu, and P. L. Richards, IEEE Trans. **MAG-25**, 1050 (1989).

[13]J. Bardeen, Phys. Rev. Lett. **6**, 57 (1961); M. H. Cohen, L. M. Falicov, and J. C. Phillips, *ibid.* **8**, 316 (1962); V. Ambegaokar and A. Baratoff, *ibid.* **10**, 486 (1963).

[14]C. A. Hamilton and S. Shapiro, Phys. Rev. Lett. **26**, 426 (1971); C. A. Hamilton, Phys. Rev. B **5**, 912 (1972).

[15]Q. Hu, C. A. Mears, P. L. Richards, and F. L. Lloyd, Phys. Rev. Lett. **64**, 2945 (1989).

[16]A. H. Dayem and R. J. Martin, Phys. Rev. Lett. **8**, 246 (1962); P. K. Tien and J. P. Gordon, Phys. Rev. **129**, 647 (1963).

[17]A. Yariv, *Quantum Electronics*, 2nd ed. (Wiley, New York, 1975), Chap. 8.

[18]D. Rogovin and D. J. Scalapino, Ann. Phys. (N.Y.) **86**, 1 (1974).

[19]P. L. Richards, T.-M. Shen, R. E. Harris, and F. L. Lloyd, Appl. Phys. Lett. **36**, 480 (1980).

[20]G. S. Lee, Appl. Phys. Lett. **41**, 291 (1982).

[21]Q. Hu, C. A. Mears, P. L. Richards, and F. L. Lloyd, IEEE Trans. **MAG-25**, 1380 (1989).

[22]R. E. Collin, *Foundations for Microwave Engineering* (McGraw-Hill, New York, 1966), Chap. 5.

[23]D. B. Rutledge, D. P. Neikirk, and D. P. Kasilingam, in *Infrared and Millimeter Waves*, edited by K. J. Button (Academic, New York, 1983), pp. 1–90.

[24]P. H. Siegel, IEEE Trans. Microwave Theory Tech. **MTT-S Digest**, 649 (1986); R. C. Compton, R. C. McPhedran, Z. Popovic, G. M. Rebeiz, P. P. Tong, and D. B. Rutledge, IEEE Trans. **AP-35**, 622 (1987).

[25]M. N. Afsar, IEEE Trans. **MTT-32**, 1598 (1984); **IM-36**, 554 (1987).

[26]W. H. Chang, J. Appl. Phys. **50**, 8129 (1979).

[27]J. H. Greiner *et al.*, IBM J. Res. Dev. **24**, 195 (1980).

[28]A. R. Kerr, S.-K. Pan, and M. J. Feldman, Int. J. Infrared Mm. Waves **9**, 203 (1988).

[29]Q. Hu, C. A. Mears, P. L. Richards, and F. L. Lloyd, Int. J. Infrared Mm. Waves **9**, 303 (1988).

[30]P. L. Richards and Q. Hu, IEEE Proc. **77**, 1233 (1989).

[31]J. E. Carlstrom, R. L. Plambeck, and D. D. Thornton, IEEE Trans. **MTT-33**, 610 (1985).

[32]P. L. Richards, in *Spectroscopic Technique for Far Infrared, Submillimeter and Millimeter Waves* (North-Holland, Amsterdam, 1967), p. 33.

[33]M. Gurvitch, M. A. Washington, and H. A. Huggins, Appl. Phys. Lett. **42**, 472 (1983).

[34]A. W. Lichtenberger, C. P. McClay, R. J. Mattauch, M. J. Feldman, S. -K. Pan, and A. R. Kerr, IEEE Trans. **MAG-25**, 1247 (1989); S. Han, J. Lapointe, and J. E. Lukens, Phys. Rev. Lett. **63**, 1712 (1989).

[35]R. J. Bell, *Introductory Fourier Transform Spectroscopy* (Academic, New York, 1972), Chap. 5.

[36]P. L. Richards and S. A. Sterling, Appl. Phys. Lett. **14**, 394 (1969).

[37]P. Seidel and J. Richter, Phys. Status Solidi **98**, 189 (1980), and references therein.

[38]A. D. Smith and P. L. Richards, J. Appl. Phys. **53**, 3806 (1982).

[39]R. L. Kautz, J. Appl. Phys. **49**, 308 (1978).

[40]L. L. Chang, L. Esaki, and R. Tsu, Appl. Phys. Lett. **24**, 593 (1974); T. C. L. G. Sollner, W. D. Goodhue, P. E. Tannenwald, C. D. Parker, and D. D. Peck, *ibid.* **43**, 588 (1983); M. Tsuchiya, T. Matsusue, and H. Sakaki, Phys. Rev. Lett. **59**, 2356 (1987).